

Effects of next-nearest-neighbor hopping on the hole motion in an antiferromagnetic background

Avraham Schiller, Pradeep Kumar, Rainer Strack, Dieter Vollhardt

Angaben zur Veröffentlichung / Publication details:

Schiller, Avraham, Pradeep Kumar, Rainer Strack, and Dieter Vollhardt. 1995. "Effects of next-nearest-neighbor hopping on the hole motion in an antiferromagnetic background." *Physical Review B* 51 (13): 8337-46. <https://doi.org/10.1103/physrevb.51.8337>.



Effects of next-nearest-neighbor hopping on the hole motion in an antiferromagnetic background

Avraham Schiller and Pradeep Kumar

*National High Magnetic Field Laboratory and Department of Physics, The University of Florida,
Gainesville, Florida 32611*

Rainer Strack and Dieter Vollhardt

Institut für Theoretische Physik C, Technische Hochschule Aachen, Templergraben 55, D-52056 Aachen, Germany

(Received 22 September 1994)

In this paper we study the effect of next-nearest-neighbor hopping on the dynamics of a single hole in an antiferromagnetic (Néel) background. In the framework of large dimensions the Green function of a hole can be obtained exactly. The exact density of states of a hole is thus calculated in large dimensions and on a Bethe lattice with large coordination number. We suggest a physically motivated generalization to finite dimensions (e.g., 2 and 3). In $d = 2$ we present also the momentum-dependent spectral function. With varying degree, depending on the underlying lattice involved, the discrete spectrum for holes is replaced by a continuum background and a few resonances at the low-energy end. The latter are the remnants of the bound states of the t - J model. Their behavior is still largely governed by the parameters t and J . The continuum excitations are more sensitive to the energy scales t and t_1 .

I. INTRODUCTION

The dynamics of a hole in an antiferromagnetic background is a physically interesting but complex problem with a long history,¹⁻⁴ in particular in the theory of magnetic semiconductors.³ In solid ³He,⁵ it precisely corresponds to the motion of vacancies at low temperatures. Due to the fact that in lightly doped high- T_c superconducting materials holes move in the antiferromagnetic background of the original undoped insulator,⁶ the problem received wide attention again, leading to exciting new physical insight. Nevertheless, a complete solution still does not exist. The theory has recently been reviewed by Yu *et al.*⁷

The physical problem is most easily understood for an Ising antiferromagnetic (i.e., Néel) background with exchange coupling J in two dimensions. As the hole moves, it breaks spin bonds. A straight-line motion over a distance x thus leads to a string of broken bonds and thus to an increase in energy proportional to Jx . At the same time strings unwind themselves if the hole moves around a loop one and a half times.⁸ Nevertheless, since the latter is a rather high-order process in the hopping amplitude t , a hole has been considered to be bound in a linear potential.^{3,9} The resulting hole spectrum consists of a sequence of discrete eigenvalues. For a t - J model these can be seen to scale with $t(J/t)^{2/3}$ from essentially dimensional arguments. Inclusion of Heisenberg-like spin-flip interactions leads in turn to delocalization of the hole and the formation of an effective quasiparticle band whose width is of the order of J . This scenario has been studied extensively in one and two dimensions using various analytic and numerical techniques.^{10-16,7}

We shall argue below that physical considerations sug-

gest an approach that involves an additional energy scale t_1 , the hopping amplitude to next-nearest-neighbor sites. A realistic band structure simply cannot be fit by an energy dispersion that originates solely from nearest-neighbor hopping.¹⁷⁻¹⁹ In fact, estimates for $|t_1/t|$ range from approximately 0.15 for $\text{La}_{2-x}\text{Sr}_x\text{CuO}_4$ to roughly 0.45 for $\text{YBa}_2\text{Cu}_3\text{O}_{7-x}$,¹⁷ indicating that t_1 is far from being a small energy scale. The significance of a t_1 term is profound. In a bipartite lattice, motion via t_1 leaves the spin configuration invariant. Hence the particle becomes free to move without having to distort the spin background. While Trugman loops⁸ can be viewed as effective t_1 processes where $t_1 \sim t^6$, we expect that a bare t_1 exists as an intermediate energy scale. We are thus led to investigate the t - t_1 - J model and to ask the question,²⁰ *how does t_1 alter the physical picture described above?*

For the t - J model the problem of a single hole in an antiferromagnetic background was recently solved in the limit of large dimensions, $d \rightarrow \infty$,²¹ by Metzner *et al.*²² for $J = 0$ and by Strack and Vollhardt^{23,24} for $J > 0$. They were able to show that string unwindings, whether because of Heisenberg-like spin-flip interactions or as a result of Trugman loop motion, become negligible in the limit of infinite d . Hence approximations such as the Brinkman-Rice retraceable path approximation⁴ (rpa) or the linear potential approach^{3,9} become exact at $d = \infty$. As a result, the density of states for a hole and its dynamical conductivity can be calculated exactly for $d = \infty$. Moreover, systematic improvements may be obtained through an expansion in powers of $1/d$.²²⁻²⁴ They show, for example, that the results of the retraceable-path approximation in *finite* dimensions correspond to a self-consistent $1/d$ -expansion of the exact $d = \infty$ result.^{23,24} Furthermore, starting from the retraceable-path approximation and resumming the Nagaoka expansion in terms

of nonretraceable skeleton paths dressed by retraceable-path insertions Müller-Hartmann and Ventura²⁵ recently obtained an almost quantitative solution of the one-particle problem in all dimensions. There is good agreement with the numerical results of Zhong *et al.*,²⁶ which were obtained for a double chain and a square lattice with a new Lanczos iteration scheme.

For the t - J model in infinite dimensions the Green function is local and satisfies a self-consistent equation²³

$$G_{ii}(z) = \left\langle i \left| \frac{1}{z - \mathcal{H}} \right| i \right\rangle = \frac{1}{z - t^{*2} G_{ii}(z - \frac{J^*}{2})}, \quad (1)$$

which may be solved explicitly in terms of Bessel functions.²⁷ Here $|i\rangle$ represents the Néel state with a hole at site i . The parameters t^* and J^* are appropriately scaled energies whose precise definition will be given below. Equation (1) coincides with the approximation by Kane *et al.*,¹⁰ the latter is therefore exact in large dimensions.

In light of its success in capturing several of the essential physical features of hole motion in the t - J model, we employ the limit of large dimensions also to the t - t_1 - J model. Exact expressions are derived for the hole Green function $G_{ij}(z)$ at $d = \infty$ and a natural extension to finite dimensions is provided. The latter continues to possess all required analytical properties, including spectral sum rules.

The paper is organized as follows: Section II contains a description of the Hamiltonian and the necessary parameter scalings for $d = \infty$. In Sec. III, we derive the Green function for holes on a hypercubic lattice in $d = \infty$, for a Bethe lattice with $Z = \infty$, and for a generalization of our results to finite d ($= 2, 3$). Section IV contains a discussion of our results, followed by a summary in Sec. V. In an appendix we address the analytical properties of our finite d generalization.

II. t - t_1 - J MODEL AND THE LIMIT OF LARGE DIMENSIONS

The Hamiltonian we consider, written for convenience in terms of creation and annihilation operators for holes, is given by

$$\begin{aligned} \mathcal{H} &= t \sum_{\langle i,j \rangle, \sigma} n_{i,-\sigma}^h h_{i\sigma}^\dagger h_{j\sigma} n_{j,-\sigma}^h \\ &+ t_1 \sum_{\langle\langle i,j \rangle\rangle, \sigma} n_{i,-\sigma}^h h_{i\sigma}^\dagger h_{j\sigma} n_{j,-\sigma}^h + J \sum_{\langle i,j \rangle} \mathbf{S}_i \cdot \mathbf{S}_j \\ &= \mathcal{H}_t + \mathcal{H}_{t_1} + \mathcal{H}_J. \end{aligned} \quad (2)$$

Here $h_{i\sigma}$ ($h_{i\sigma}^\dagger$) annihilates (creates) a hole with spin σ on site i , and \mathbf{S}_i is the spin at site i . The operators $n_{i,\sigma}^h = h_{i\sigma}^\dagger h_{i\sigma}$, which appear in the hopping terms, ensure that no *electronic* double occupancy occurs in the course of hopping. As always, $\langle i, j \rangle$ denotes nearest-neighboring sites, while the notation $\langle\langle i, j \rangle\rangle$ represents next-nearest neighbors.

We adopt Eq. (2) as our basic model, whose micro-

scopic justification traces back to the Hubbard model with a next-nearest-neighbor hopping term added. Upon carrying out the standard canonical transformation for a large U and low hole dopings,²⁸ a number of terms are generated. In addition to the J term ($J = 4t^2/U$) specified above, we recover an antiferromagnetic coupling $J_1 = 4t_1^2/U$ between next-nearest-neighbor spins, as well as a number of three-site terms. The latter include also processes where t and t_1 hoppings are combined. Clearly, a strong enough J_1 coupling will lead to frustration in the low-temperature antiferromagnetic order at half filling. Yet, by focusing on the physical range where t constitutes an energy scale larger than t_1 , the role of J_1 is mainly to renormalize the effective coupling constant J .²⁹ We therefore incorporate these effects in Eq. (2) into the (independent) parameter J . At the same time, for large U , t_1 itself may very well be *appreciably larger* than J .

Figure 1 depicts the hole trajectories in the antiferromagnetic background which become important in the presence of a t_1 term. Here we are considering paths that bring the hole back to its starting position without altering the spin configuration. The most significant contribution arises from paths shown schematically in Fig. 1(a), since they leave the spin configuration invariant. At the same time a new type of loop motion, sketched in Fig. 1(b), appears. Here, by combining two t and one t_1 hoppings, a single triangular loop motion is sufficient to restore the antiferromagnetic background. This must be compared with the case for $t_1 = 0$, where

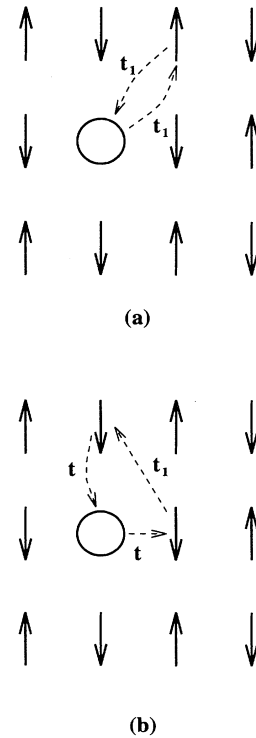


FIG. 1. Hole trajectories that become important in the presence of a t_1 term. (a) Diagonal motion; (b) triangular loop motion.

three circulations around a plaquette are necessary for the ordinary Trugman loops.

Next we introduce the limit of large dimensions. At large d the model parameters are scaled so that^{21–23}

$$t = \frac{t^*}{\sqrt{2d}}, \quad t_1 = \frac{t_1^*}{d}, \quad J = \frac{J^*}{2d}. \quad (3)$$

Keeping t^* , t_1^* , and J^* fixed, a meaningful $d \rightarrow \infty$ limit emerges. One consequence of such a limit is that spin-flip processes become negligible, so that spins may be regarded as being Ising like.²³ In addition, without t_1 , only retraceable paths are allowed up to $O(1/d^4)$.²² Now, however, both paths displayed in Fig. 1 yield nonvanishing contributions since, for example, hopping on a triangular loop [see Fig. 1(b)] is proportional to $t^2 t_1 \sim 1/d^2$, while the number of different embeddings for this path is proportional to d^2 , such that the product of the two remains of order unity even when d approaches infinity. More generally, by an appropriate combination of t and t_1 processes (or using only t_1 processes) the hole can now move on *closed loops of arbitrary length* even in $d = \infty$. Obviously the resulting motion of the hole, consisting of simple, retraceable paths and t_1 -generated, background restoring loops, can be very complex.

III. GREEN FUNCTION FOR HOLES

The hole Green function is given by

$$G_{ij}(z) = \left\langle i \left| \frac{1}{z - \mathcal{H}} \right| j \right\rangle. \quad (4)$$

Clearly i and j in Eq. (4) must lie on the same spin sublattice (taken hereafter to be the spin-up sublattice); otherwise, G_{ij} trivially vanishes.

Typically, $G_{ij}(z)$ is calculated using Nagaoka's path formalism.^{2,4} In this formulation $(z - \mathcal{H})^{-1}$ is expanded in powers of \mathcal{H}/z , and the different contributions are identified with all the different background restoring paths that extend from site j to site i . Later on we will indeed return to this approach, but first we wish to account for the fact that motion via t_1 alone is completely unrestricted. For this purpose it is useful to construct two complementary projection operators:

$$\Sigma_{ij}(z) = \langle i | \hat{\Sigma}(z) | j \rangle = t^2 \sum_{\langle i, k \rangle} \sum_{\langle j, l \rangle} \left\langle i \left| h_{i\uparrow}^\dagger h_{k\uparrow} \frac{1}{z - \mathcal{Q}(\mathcal{H}_t + \mathcal{H}_{t_1} + \mathcal{H}_{J_z}) \mathcal{Q}} h_{l\uparrow}^\dagger h_{j\uparrow} \right| j \right\rangle. \quad (10)$$

Next, as usual in $d = \infty$, $\Sigma_{ij}(z)$ becomes site diagonal.²¹ This characteristic large dimension feature follows from the application of Nagaoka's path formalism to (10). A typical path describing $\Sigma_{ij}(z)$ begins with an excitation of the ground-state spin configuration at site j , and its restoration only at the final step when the hole reaches site i . In between, the spin background is continuously excited during the entire hole motion. Consider now the case where i and j are two different sites (Fig. 2). Then

$$\mathcal{P} = \sum_{i \in \uparrow} |i\rangle \langle i|, \quad \mathcal{Q} = 1 - \mathcal{P}. \quad (5)$$

Here the summation over i is confined to the spin-up sublattice. The hole Green function (4) corresponds then to the operator

$$\hat{G}(z) = \mathcal{P} \frac{1}{z - \mathcal{H}} \mathcal{P}. \quad (6)$$

The latter may be expressed, with the aid of a familiar operator identity,³⁰ as

$$\hat{G}(z) = \frac{1}{\hat{G}^{(0)-1}(z) - \hat{\Sigma}(z)} \mathcal{P}, \quad (7)$$

where

$$\hat{G}^{(0)}(z) = \frac{1}{z - \mathcal{H}_{pp}}, \quad \hat{\Sigma}(z) = \mathcal{H}_{pq} \frac{1}{z - \mathcal{H}_{qq}} \mathcal{H}_{qp} \quad (8)$$

and

$$\mathcal{H}_{pp} = \mathcal{P} \mathcal{H} \mathcal{P}, \quad \mathcal{H}_{qq} = \mathcal{Q} \mathcal{H} \mathcal{Q}, \quad \text{etc.} \quad (9)$$

Here $\hat{G}^{(0)}(z)$ accounts for all pure t_1 processes, while all processes involving t are incorporated in the form of a self-energy. This separation into spin ground-state processes and those involving spin excitations is very useful in simplifying the algebra. For example, \mathcal{H}_{pq} and \mathcal{H}_{qp} in the numerator of $\hat{\Sigma}(z)$ necessarily require only \mathcal{H}_t and \mathcal{H}_{J_z} . However, in the denominator, \mathcal{H}_{qq} contains all processes where the hole moves in an excited spin state, including motion via t_1 .

A. Self-energy at large dimensions

Physically, all the complexity of the hole dynamics is contained within the self-energy. Yet, at finite dimensions (i.e., $d = 2, 3$), a complete solution for $\Sigma_{ij}(z)$ remains out of reach. We show, by contrast, that the problem can be solved exactly at infinite dimensions, due to a sequence of simplifications. Primarily the direct effect of spin flips on the motion of the hole vanishes as $d \rightarrow \infty$,^{22,23} and hence the self-energies can be rewritten as

the fact that the spin background is eventually restored at a site i different than j demands that the latter must be revisited by the traveling hole at some intermediate step. Otherwise, the down spin it acquired in the initial step will never be mended, as it should, to an up spin. Since the overall spin background remains excited through all intermediate stages, this implies that some other site f on the spin-up sublattice is forced to acquire a down spin, in between the two hole visits to site j .

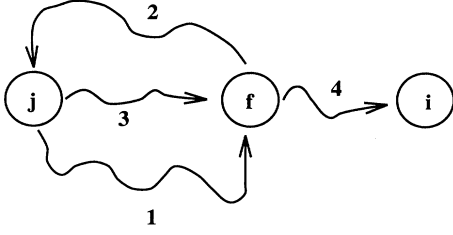


FIG. 2. A schematic description of the paths that contribute to the off-diagonal self-energy Σ_{ij} . The hole starts its motion at site j . It approaches the intermediate site f for the first time (segment 1) before revisiting site j (segment 2). Then it completes its motion to site i by way of f (segments 3 and 4).

Moreover, after the spin at site j is finally corrected to an up one, site f has to be revisited in the course of restoring the ground-state spin configuration. A schematic description of the path is shown in Fig. 2. It consists, among other things, of at least three segments where the hole propagates between the initial site j and the intermediate site f . From the standpoint of large dimensions this is two segments too many. Thus the effect of the spin background on the off-diagonal components of the self-energy is to reduce their contribution by an integer power of $1/d^2$. Indeed the path illustrated in Fig. 2 does not have the topology of a “loop tree”²² and hence does not contribute at $d = \infty$.

The third and final simplification at large dimensions occurs in the calculation of the remaining on-site self-energy. In order to evaluate $\Sigma_{ii}(z)$ we focus on the functions

$$\Sigma_{ii}^{(k,l)}(z) = \left\langle i \left| h_{i\uparrow}^\dagger h_{k\uparrow} \frac{1}{z - \mathcal{Q}(\mathcal{H}_t + \mathcal{H}_{t_1} + \mathcal{H}_{J_z}) \mathcal{Q}} h_{i\uparrow}^\dagger h_{i\uparrow} \right| i \right\rangle \quad (11)$$

(k, l being nearest neighbors of i), and compare them with

$$G_{kl}(z) = \left\langle \text{Néel} \left| h_{k\downarrow} \frac{1}{z - (\mathcal{H}_t + \mathcal{H}_{t_1} + \mathcal{H}_{J_z})} h_{i\downarrow}^\dagger \right| \text{Néel} \right\rangle. \quad (12)$$

Here |Néel) designates the antiferromagnetic spin ground state with no holes present. Equation (12) is none other than the hole Green function, only written in terms of a hole in the down-spin sublattice rather than the up-spin one. $\Sigma_{ii}^{(k,l)}(z)$ and $G_{kl}(z)$ differ in two respects: (1) The \mathcal{Q} projection operator appears in the denominator of Eq. (11), and (2) the spin at site i is flipped in Eq. (11) to a down spin. Both differences are conveniently accounted for in the limit of large dimensions by resorting once again to Nagaoka’s path formalism, and pursuing the same line of reasoning as before. Here one can see that all possible hole trajectories where site i is involved are reduced by an integer power of $1/d$ for both $\Sigma_{ii}^{(k,l)}(z)$ and $G_{kl}(z)$. Hence the spin at site i may be regarded as being *frozen* in each of the two cases. Such an observation

yields profound consequences. To begin with, the down spin at site i in the case of $\Sigma_{ii}^{(k,l)}(z)$ ensures that the spin background remains constantly excited. Therefore the \mathcal{Q} projection operators entering Eq. (11) are automatically satisfied. In addition, since apart from the flipped spin at site i the initial and final spin configurations in Eq. (11) are identical to those of Eq. (12), we precisely recover the same path contributions for both cases. Thus the *only* distinction between the two cases exists in their Ising energy, which happens to be $J^*/2$ larger for $\Sigma_{ii}^{(k,l)}(z)$. This is a result of the broken bonds between the flipped spin at site i and its surrounding nearest-neighbor spins. All in all we arrive at the following relation, which becomes exact for large dimensions:

$$\Sigma_{ii}^{(k,l)}(z) = G_{kl} \left(z - \frac{J^*}{2} \right). \quad (13)$$

Finally, the combination of Eqs. (10) and (13) yields

$$\Sigma(z) \equiv \Sigma_{ii}(z) = t^2 \sum_{\langle i,k \rangle} \sum_{\langle i,l \rangle} G_{kl} \left(z - \frac{J^*}{2} \right). \quad (14)$$

Note that no restrictions on the nature of the underlying lattice were involved in the derivation of Eq. (14); hence, it equally applies to *all* bipartite lattices in the limit of an infinite number of nearest neighbors.

B. Hole Green function at large dimensions: Hypercubic lattice

After establishing that the self-energy is site diagonal, Eq. (7) is readily solved for a hypercubic lattice by Fourier transformation:

$$G_{\mathbf{k}}(z) = \frac{1}{z - \epsilon_{\mathbf{k}} - \Sigma(z)}, \quad (15)$$

with

$$\epsilon_{\mathbf{k}} = 2t_1 \sum_{n \neq m} \cos(k_n) \cos(k_m). \quad (16)$$

Here \mathbf{k} lies within a reduced Brillouin zone, and the lattice constant is taken to be unity. The spatial Green functions are obtained from the inverse transform of Eq. (15). It yields

$$G_{ij}(z) = G_{ij}^{(0)}(z - \Sigma(z)), \quad (17)$$

where $G_{ij}^{(0)}$ is the free, tight-binding Green function due to next-nearest-neighbor hopping. Next we make use of the cubic symmetry, and express $\Sigma(z)$ from Eq. (14) as

$$\Sigma(z) = t^{*2} \left\{ G \left(z - \frac{J^*}{2} \right) + 2(d-1)G_1 \left(z - \frac{J^*}{2} \right) + G_2 \left(z - \frac{J^*}{2} \right) \right\}. \quad (18)$$

Here the notation $G \equiv G_{ii}$ and G_1 was introduced for the on-site and next-nearest-neighbor Green functions, respectively, while G_2 corresponds to the case where the two lattice sites lie on the same axis, yet with a separation of two lattice constants (i.e., third-order nearest neighbors). The former two functions are further related through an identity that links the corresponding local and next-nearest-neighbor tight-binding Green functions. Indeed for any dimension

$$2(d-1)G_1^{(0)}(z) = \frac{zG^{(0)}(z) - 1}{t_1^*}, \quad (19)$$

where $G_{ii}^{(0)} \equiv G^{(0)}$. Thus, since $G_2(z)$ vanishes at large dimensions as $1/d$, Eqs. (18) and (19) reduce at the limit of $d \rightarrow \infty$ to

$$\Sigma(z) = t^{*2} \left\{ G\left(z - \frac{J^*}{2}\right) + \frac{[z - \frac{J^*}{2} - \Sigma(z - \frac{J^*}{2})]G(z - \frac{J^*}{2}) - 1}{t_1^*} \right\}. \quad (20)$$

Together, Eqs. (17) and (20) combine to give an iterative equation for the local Green function $G(z)$, which is exact at $d = \infty$. It must be supplemented, however, with the corresponding $d = \infty$ expression for $G^{(0)}(z)$ which may be obtained (using the corresponding density of states³¹) as³²

$$G^{(0)}(z) = \frac{-i}{2t_1^*} \frac{\sqrt{\pi}}{\sqrt{(z+t_1^*)/2t_1^*}} W\left(\sqrt{\frac{z+t_1^*}{2t_1^*}}\right). \quad (21)$$

Here $W(z)$ is the scaled complementary error function of a complex argument,³³ and the sign of the square root is chosen so that it lies in the upper half plane.

C. Hole Green function on a Bethe lattice

In case of a Bethe lattice, the definitions of the scaled parameters are modified as

$$t = \frac{t^*}{\sqrt{Z}}, \quad t_1 = \frac{t_1^*}{Z}, \quad J = \frac{J^*}{Z}, \quad (22)$$

where Z is the coordination number. Once these adjustments are carried out, Eqs. (17) and (20) continue to hold as the exact $Z = \infty$ equations for the hole Green function $G_{ij}(z)$ where now, however, $G^{(0)}(z)$ in Eq. (20) is given by⁴

$$G^{(0)}(z) = \frac{1 - \sqrt{1 - 4t_1^*/(z+t_1^*)}}{2t_1^*}. \quad (23)$$

D. Extension to finite dimensions

A systematic $1/d$ expansion about the $d = \infty$ limit constitutes in general a formidable task, and in that respect the problem of hole motion in the t - t_1 - J model is no exception. Here we consider a hypercubic lattice

and suggest an alternative, approximate way to bridge between $d = \infty$ and finite d .

We base our approach on the same equations that were derived for large dimensions, yet by two adjustments. First, the $G_{ij}^{(0)}(z)$ Green functions are replaced by their corresponding d -dimensional expressions. Second, we retain the contribution of G_2 to the local self-energy, i.e., use Eq. (18) rather than Eq. (20). Though the latter contribution completely vanishes as $d \rightarrow \infty$, it is essential to keep it at finite d in order to avoid a nonphysical spectral function (note that for $d < \infty$ a shift occurs in the band edge of the spectral part of $G^{(0)}(\omega - i\delta)$; see, e.g., Fig. 3). We elaborate on this point in the Appendix. The complete set of equations employed for a finite d consists, therefore, of Eq. (17), together with the following version of Eq. (18):

$$\Sigma(z) = t^{*2} \left\{ G\left(z - \frac{J^*}{2}\right) + \frac{(z - \frac{J^*}{2} - \Sigma(z - \frac{J^*}{2}))G(z - \frac{J^*}{2}) - 1}{t_1^*} + G_2\left(z - \frac{J^*}{2}\right) \right\}. \quad (24)$$

We further note that the only input function required at $d = \infty$ is $G^{(0)}(z)$, while for a finite d it is joined by $G_2^{(0)}(z)$. For $d = 2, 3$, both functions can be computed using complete elliptic integrals of the first and second kinds, provided they are properly continued to the entire complex plane.³⁴ In the Appendix we show that all analytical properties required from $G_{ij}(z)$ are indeed conserved within the approximation scheme suggested above.

IV. NUMERICAL RESULTS

A. Bare density of states

Figure 3 shows the bare density of states (DOS) due to pure t_1 hopping on a hypercubic lattice in $d = 2, 3, \infty$, and on a Bethe lattice with an infinite coordination number $Z = \infty$.

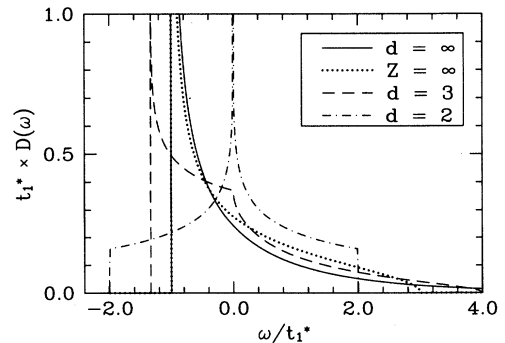


FIG. 3. Bare DOS due to pure t_1 hopping on a hypercubic lattice in $d = 2, 3, \infty$, and on a Bethe lattice with an infinite coordination number $Z = \infty$.

responding to the DOS for a square lattice, in $d = 3$ and $d = \infty$ [see Eq. (21)], corresponding to the DOS for a fcc lattice in those dimensions, and, finally, for a Bethe lattice with $Z = \infty$, Eq. (23). There is a divergence at the lower band edge (for $t_1^* > 0$), either with a square root singularity for $d = \infty$ and the Bethe lattice, or in a logarithmic manner³⁴ for $d = 3$. For $d = 2$ the logarithmic singularity is at the band center. The curves for $d = \infty$ and Bethe lattice are clearly very similar, although the bandwidth for a Bethe lattice remains finite. In contrast, $d = \infty$ possesses an exponential tail that extends to higher energies.³¹ For $d = 2$ and 3 there is a slight shift in the lower band edge as mentioned earlier in Sec. IIID. Except for $d = 2$ the cases look qualitatively similar. For $t_1^* < 0$ the bare density of states is inverted (i.e., $\omega \rightarrow -\omega$). The divergences then move to the upper band edge, with the exception of the $d = 2$ case which is symmetric in ω .

B. Infinite dimensions

Figure 4 shows the effect of an increase in $t_1^* > 0$ on the DOS for the motion of a hole in the infinite-dimensional t - t_1 - J model at fixed $J^*/t^* = 0.4$. For $t_1^*/t^* = 0.05$ we see only minor changes from the case where $t_1^* = 0$: There are new satellites in between the original bound state energies, starting at $\omega_0 + J^*/2$, where ω_0 is the lowest bound state energy; the sharp δ peaks for $t_1^* = 0$ have now acquired a small width. (Note, however, that we expect the realistic energy hierarchy to be $t^* > t_1^* \gtrsim J^*$.) At $t_1^*/t^* = 0.2$ a continuous spectrum has developed. The sharp structures near the lower band edge are derived from the divergence of the bare DOS. At $t_1^*/t^* = 0.4$

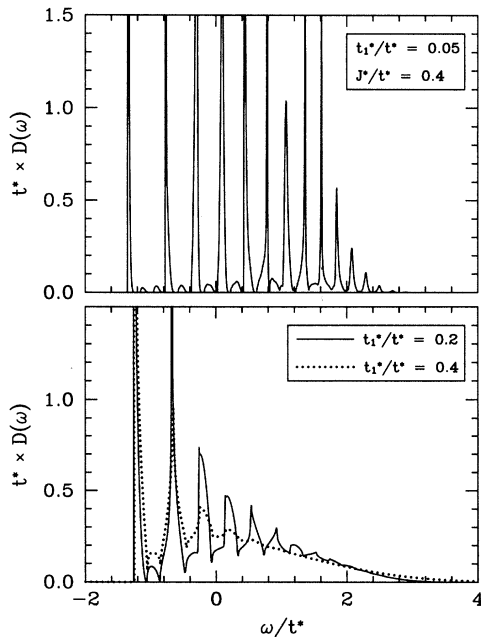


FIG. 4. DOS for $J^*/t^* = 0.4$ and $t_1^*/t^* = 0.05, 0.2$, and 0.4 for a hypercubic lattice at $d = \infty$.

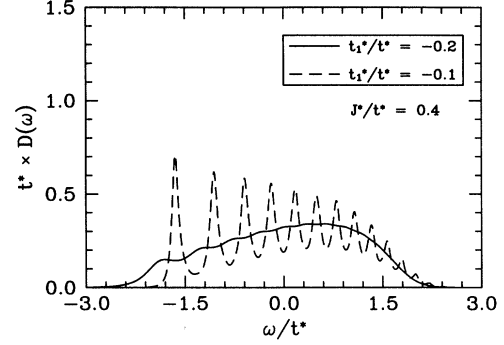


FIG. 5. Similar to Fig. 4, but with $t_1^*/t^* = -0.1$ and -0.2 . Notice the disappearance of all discrete (resonant) structures for $t_1^*/t^* = -0.2$.

only the lowest resonances appear discernible. The rest has been absorbed into the incoherent continuum of excitations. Any further increase in t_1^* leads to additional decrease of the resonant peaks and a further development of the underlying continuum. It looks as if one is approaching the general shape of the bare (continuous) density of states.

For $t_1^* < 0$, Fig. 5, there is a dramatic change in the DOS. By $t_1^*/t^* = -0.2$ only weak traces are left of the bound states at $t_1^* = 0$. The DOS is more symmetric and less structured compared to $t_1^* > 0$. It corresponds to an incoherent band with an exponentially small tail that extends to negative energies. The origin of the strong effect that a negative t_1^* has on the hole motion lies in the unboundedness of the bare DOS for $\omega \rightarrow -\infty$. As a result, the self-energy acquires a nonzero imaginary part throughout the negative energy region.

Figure 6 displays the DOS for a Bethe lattice with

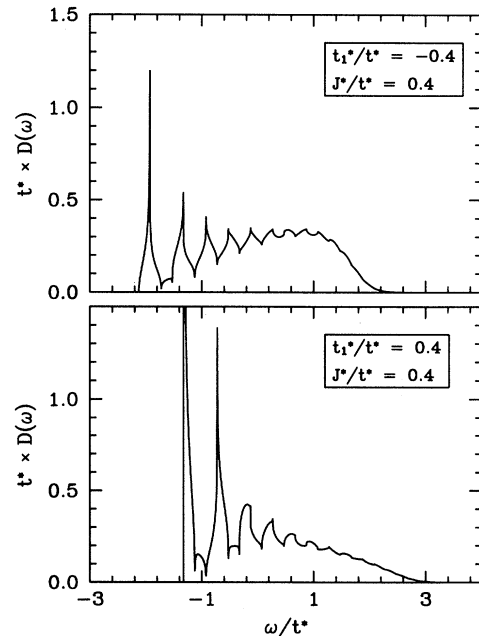


FIG. 6. Bethe lattice with coordination number $Z = \infty$: DOS for $J^*/t^* = 0.4$ and $t_1^*/t^* = \pm 0.4$.

$Z = \infty$ for $J^*/t^* = 0.4$ and $t_1^*/t^* = \pm 0.4$. Again, well-developed incoherent continua are recovered, similar to the ones obtained for $d = \infty$. The resonances persist, however, even for $t_1^*/t^* = -0.4$. They seem to be the dominant structures for smaller values of $|t_1^*|$ ($|t_1^*| \lesssim 0.2$). Notice also the shift in the threshold energy between $t_1^* > 0$ and $t_1^* < 0$. For $t_1^* < 0$ the resonances shift to lower energies with increasing $|t_1^*|$, while in case of $t_1^* > 0$ the lower edge is quite insensitive to variations in t_1^* . The difference between $d = \infty$ and the Bethe lattice is mostly due to the finite width of the bare spectrum of the latter.

C. Finite dimensions

Next we turn to finite dimensions. Figure 7 depicts our generalization to $d = 3$ for $J^*/t^* = 0.4$ and $t_1^*/t^* = \pm 0.2, \pm 0.4$. The width and magnitude of the incoherent spectra seem to be similar for $t_1^* < 0$ and $t_1^* > 0$, as for all lattices discussed here. The lower edge is found, once again, to have no significant shift with t_1^* for $t_1^* > 0$, while it decreases with decreasing t_1^* for $t_1^* < 0$. The qualitative behavior of the DOS for $t_1^*/t^* = 0.4$ is similar to that obtained by Bala *et al.*²⁰ for $d = 2$ using a very different method. The effect of a smaller J^* , corresponding to what might be expected for realistic material parameters, is shown in Fig. 8; for $J^*/t^* = 0.1$ and $t_1^*/t^* = -0.4$, we recover a broad incoherent spectrum. At the same time, resonances can be clearly seen at the lower edge, with widths that are smaller than the separation between adjacent peaks. The low-energy features thus persist even for J^* appreciably smaller than t_1^* .

We now examine more closely the low-energy spectrum for two dimensions. For $d = 2$, the general features described above are seen as well. The effect of increasing $|t_1^*|$

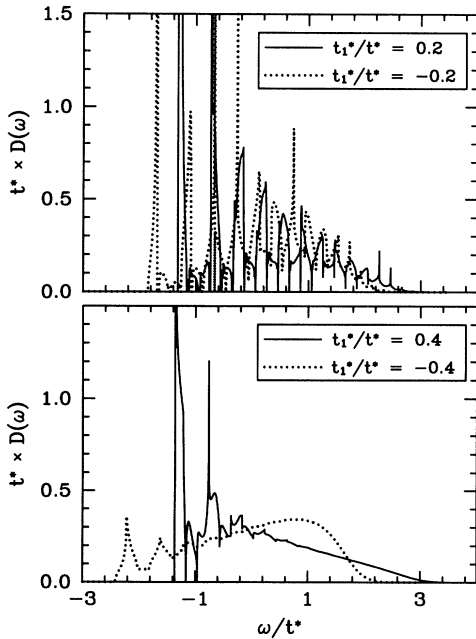


FIG. 7. DOS in $d = 3$ [see Eq. (24)]: DOS for $J^*/t^* = 0.4$ and $t_1^*/t^* = \pm 0.2, \pm 0.4$.

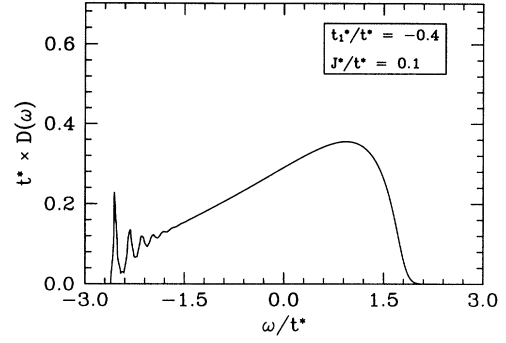


FIG. 8. Same as Fig. 7 with $J^*/t^* = 0.1$ and $t_1^*/t^* = -0.4$.

is to broaden the original bound states into resonances, eventually leading to a continuum in the DOS. There are, however, two major differences. The first is that a larger $|t_1^*|$ is needed to produce qualitatively similar results in $d = 2$, as compared to $d = 3$. The reason is simple: The overall bandwidth of the bare DOS is smaller for $d = 2$ (see Fig. 3). The other difference is that in $d = 3$ a negative t_1^* is seen to be more effective in smearing out the residual details of the bound states. In $d = 2$, the roles are slightly inverted. This has to do with the symmetric character of the bare DOS in $d = 2$ as opposed to the strong asymmetry for $d \geq 3$.

We have also studied the \mathbf{k} -dependent spectral function $A(\mathbf{k}, \omega)$ for $d = 2$. Figure 9 shows $A(\mathbf{k}, \omega)$ for $\mathbf{k} = (\frac{\pi}{2}, \frac{\pi}{2})$ and $J^*/t^* = 0.2$, $t_1^*/t^* = -0.6$. It looks quite similar to the spectral function calculated numerically by Liu and Manousakis¹² for the t - J model on a finite-size lattice ($J^*/t^* = 0.2$ corresponds, for $d = 2$, to $J/t = 0.1$). The lowest peak in this curve corresponds to a coherent state. Indeed *all* \mathbf{k} states within a margin of $J^*/2$ from the lower band edge have vanishing imaginary part of the self-energy. Physically, this corresponds to their inability to decay by emitting or absorbing spin excitations, which is a consequence of the Ising nature of the spins. For $t_1^* < 0$ the dispersion of this coherent band is similar to that of the bare energy in Eq. (16), with a strong renormalization due to J^* . To be more specific, we find that

$$E(\mathbf{k}) = \frac{J^*}{2} f(\mathbf{k}; t_1^*) + \text{const.} \quad (25)$$

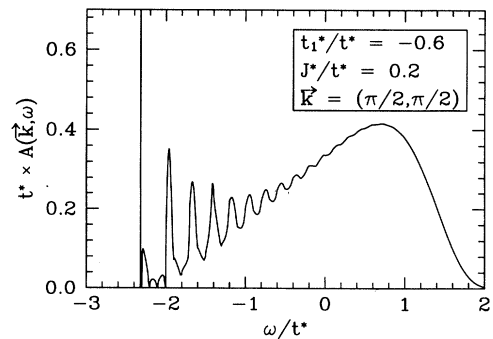


FIG. 9. The $A(\mathbf{k}, \omega)$ spectral function for $d = 2$ and $\mathbf{k} = (\frac{\pi}{2}, \frac{\pi}{2})$. Here $J^*/t^* = 0.2$ and $t_1^*/t^* = -0.6$.

For a fixed t_1^* and different J^* , the eigenvalues scale with $J^*/2$ in that $[E(\mathbf{k}) - E(\mathbf{k}_0)] / \left(\frac{J^*}{2}\right)$ all lie on the same curve. This is demonstrated in Fig. 10(a). The function f , however, differs from Eq. (16) in that the upper band edge is deformed towards lower energies for non-negligible values of t_1^* [see Fig. 10(b)]. For small values of t_1^* , though, f is essentially linear in t_1^* . The overall integrated spectral weight of the entire band can be expressed as

$$\int d\epsilon_{\mathbf{k}} \rho^{(0)}(\epsilon_{\mathbf{k}}) \frac{dE(\mathbf{k})}{d\epsilon_{\mathbf{k}}}, \quad (26)$$

where $\rho^{(0)}$ is the bare DOS for $d = 2$. Following $E(\mathbf{k})$, Eq. (26) also scales with J^* . One consequence of the self-energy being \mathbf{k} independent in our approximation is that the minimum of $E(\mathbf{k})$ always occurs at the Γ point, $\mathbf{k} = (0, 0)$.

For positive t_1^* in $d = 2$, one notable feature is that for moderate t_1^* ($t_1^* \lesssim J^*$), when the low-energy resonance in the DOS has almost become part of the continuum, there are wave vectors for which coherent state solutions no longer exist. Three types of solutions are then recovered. At low frequencies, and over a frequency range of $\Delta\omega = J^*/2$, true coherent state solutions are found. These are centered around the band minima at $\mathbf{k} = (\pi, 0)$. At slightly higher frequencies, the imaginary part of the self-energy becomes nonzero in a quadratic manner. The solutions are thus quasiparticle like. In the neighborhood of $\mathbf{k} = (0, 0)$ —the upper band edge—and over an area in \mathbf{k} space that increases with increasing t_1^* , the solutions are removed from the low-energy side and

are shifted to the incoherent high-frequency side of the spectrum.

V. DISCUSSION

In this paper we explored the consequences of a next-nearest-neighbor hopping t_1 on the motion of a single hole in a quantum antiferromagnet. The system is described by a t - t_1 - J model. Our motivation stems both from the need of a t_1 term to characterize the observed electronic structure,^{17–19} and from the growing numerical evidence³⁵ that the effective quasiparticle dispersion generated by the t - J model can be parametrized by means of effective next-nearest-neighbor and third-order nearest-neighbor hops. Our approach is based on the limit of large dimensions, where the problem is solved exactly. For $d = \infty$, t_1 survives as the *only* mechanism that delocalizes the hole. The principal effect of the introduction of t_1 is thus seen in the following steps: (a) For $t_1^* = 0$ (and $J^* \neq 0$), we have only bound states that are typically separated by $t(J/t)^{2/3}$; (b) as t_1^* increases ($t_1^* \ll J^*$), all peaks in the density of states acquire width, and satellites appear at intermediate energies $\epsilon_{n,m} = \omega_n + a_{n,m}J^*/2$ [here ω_n is the energy of the n th bound state and $a_{n,m} \sim O(1)$]; (c) as t_1^* further increases ($t_1^* \sim J^*$), the satellites and resonant peaks merge, and a continuum is formed. Hence t_1 restores the incoherent Brinkman-Rice⁴ spectra at high energies, while generating a quasiparticle dispersion at low energies. This is most clearly seen within our analysis in $d = 2$. For $|t_1^*| \ll J^*$ and ω close to the low-energy edge, we may replace the self-energy in Eq. (17) with its $t_1^* = 0$ limit. Then, using a dominant pole approximation,¹⁰

$$G_{\mathbf{k}}(\omega + i\delta) \cong \frac{Z_0}{\omega - \omega_0 - Z_0\epsilon_{\mathbf{k}}}, \quad (27)$$

where ω_0 and Z_0 are the $t_1^* = 0$ ground-state energy and quasiparticle amplitude, respectively. Hence a quasiparticle band immediately appears, with a characteristic renormalization Z_0 . Its bandwidth is given by $4Z_0t_1^*$ (the factor 4 is for $d = 2$), while the \mathbf{k} -independent effective mass is proportional to $1/(Z_0t_1^*)$. The effect of J^* enters via the quasiparticle amplitude Z_0 . In the intermediate and large regimes for t_1^*/J^* , the bandwidth is practically governed by J^* (see, e.g., Fig. 10). For $t_1^* < 0$, the entire Brillouin zone is included in this band, and the quasiparticle dispersion scales with J^* . At moderate values of $t_1^* > 0$, quasiparticle solutions are removed from the vicinity of the Γ point. In both cases, the frequency range of width $J^*/2$ at the lowest band edge accommodates only coherent states. This corresponds to the inability of holes to lose energy by flipping the spins. The latter is a consequence of large dimensions where the original Heisenberg spins become Ising like; i.e., quantum spin fluctuations are suppressed. Quantum fluctuations are known to have two important effects in the t - J model. Together with Trugman loops⁸ they act to delocalize the hole, giving rise to an effective quasiparticle energy dispersion that can be fitted by effective

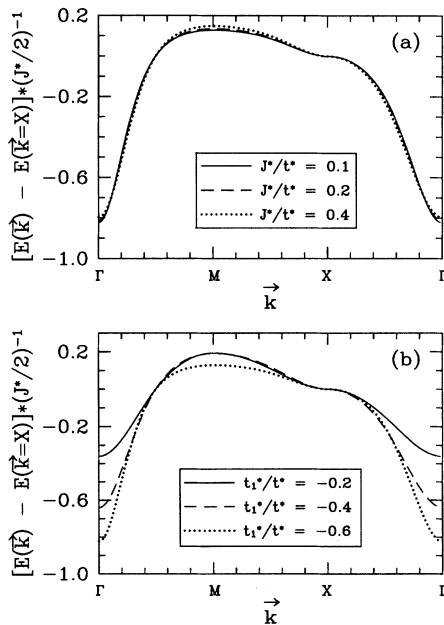


FIG. 10. The quasiparticle dispersion $E(\mathbf{k})$ for $d = 2$, (a) as a function of J^* for fixed $t_1^*/t^* = -0.6$, (b) as a function of t_1^* for fixed $J^*/t^* = 0.1$. Here $\Gamma = (0, 0)$, $M = (\pi, 0)$, and $X = (\frac{\pi}{2}, \frac{\pi}{2})$.

hops to next-nearest-neighbor and third-order nearest-neighbor sites. Quantum fluctuations are also responsible for the quasiparticle-band minimum at $\mathbf{k} = (\frac{\pi}{2}, \frac{\pi}{2})$ (see, e.g., Zhou and Schultz¹⁶ for a clear demonstration of this point). The introduction of a t_1 term to the model, motivated by physical considerations, simulates quite well the dispersion, i.e., delocalization, of the hole but cannot produce a band minimum at $\mathbf{k} = (\frac{\pi}{2}, \frac{\pi}{2})$.

In summary, we have provided a simple analytic theory for the hole motion in an antiferromagnetic background in the presence of next-nearest-neighbor hopping. The theory is exact in the limit of large dimensions. In finite dimensions it provides a useful mean-field description of this physically relevant phenomenon.

ACKNOWLEDGMENTS

Two of us (A.S. and P.K.) are grateful to L. Borkowski for stimulating discussions at early stages of this work. D.V. acknowledges a useful discussion with P. Horsch. This work was supported by the NHMFL (A.S. and P.K.), DOE Grant No. DE-FG05-91ER45462 (P.K.), and the Deutsche Forschungsgemeinschaft through Sonderforschungsbereich 341 (R.S. and D.V.).

APPENDIX

In this appendix we show that our generalization to finite dimensions, Eq. (24), retains all analytical properties in the upper and lower half planes, as required of $G_{ij}(z)$. Our strategy is as follows: First we show that the imaginary parts of $\Sigma(z)$ and z have opposite signs, which implies that z and $z - \Sigma(z)$ always lie in the same half plane. In particular, $z - \Sigma(z)$ never crosses the real axis, unless z becomes purely real. Then, making use of the known analytical structure of $G_{ij}^{(0)}(z)$ we conclude that (1) $G_{ij}(z) = G_{ij}^{(0)}(z - \Sigma(z))$ has no poles in either the upper or lower half planes; (2) $\text{Im } G(z)$ has a fixed sign throughout each of the two half planes. The latter point guarantees that the spectral part of G is non-negative. Finally, the spectral sum rule (i.e., the normalization of the spectral function to unity) is a direct consequence of the fact that $G(z)$ falls like $1/z$ for large $|z|$ and has no poles outside the real axis.

We now construct the first and principal step in the procedure outlined above. From the asymptotic behavior of $G_{ij}^{(0)}(z)$ it follows that $G(z) = G^{(0)}(z - \Sigma(z))$ falls like $1/z$ for large $|z|$, while $G_1(z)$ and $G_2(z)$ decay according to higher powers of $1/z$. Thus, by virtue of Eq. (18),

$\Sigma(z) \sim \frac{t^{*2}}{z}$ for $|z| \rightarrow \infty$. Asymptotically it is therefore apparent that the imaginary parts of $\Sigma(z)$ and z acquire opposite signs. This relation can now be extended to the entire upper and lower half planes using the recursion relation, Eq. (18). Replacing $G(z)$, $G_1(z)$, and $G_2(z)$ with explicit k -space integrations, Eq. (18) is rewritten as

$$\Sigma\left(z + \frac{J^*}{2}\right) = \int_{-\pi}^{\pi} \prod_{l=1}^d \frac{dk_l}{2\pi} \frac{t^{*2}}{z - \Sigma(z) - \epsilon_{\mathbf{k}}} \times \left\{ 1 + \frac{2}{d} \sum_{n \neq m} \cos(k_n) \cos(k_m) + \frac{1}{d} \sum_{n=1}^d \cos(2k_n) \right\}. \quad (\text{A1})$$

Here the different terms in the curly brackets correspond to $G(z)$, $G_1(z)$, and $G_2(z)$, respectively. These may be easily brought to the form

$$\Sigma\left(z + \frac{J^*}{2}\right) = \frac{2t^{*2}}{d} \int_{-\pi}^{\pi} \prod_{l=1}^d \frac{dk_l}{2\pi} \frac{\left[\sum_{n=1}^d \cos(k_n)\right]^2}{z - \Sigma(z) - \epsilon_{\mathbf{k}}}, \quad (\text{A2})$$

which clarifies the positivity of the numerator in the integrand. Explicitly taking the imaginary part of the right-hand side in Eq. (A2), we find that $\text{Im } \Sigma(z + \frac{J^*}{2})$ and $\text{Im } \{z - \Sigma(z)\}$ always have opposite signs. Thus, given that asymptotically $\text{Im } \Sigma(z)$ is negative (positive) in the upper (lower) half plane, and since any point in the half plane can be approached from the asymptotic regime by way of repeated applications of the recursion relation, $\text{Im } \Sigma(z)$ remains negative (positive) throughout the entire half plane. Hence the imaginary parts of z and $\Sigma(z)$ always acquire opposite signs.

Having established this point, the analytical properties of $G_{ij}(z)$ follow along the lines illustrated above. Both the positivity of the spectral function and the spectral sum rule have also been confirmed numerically for several cases, including those displayed in Figs. 7, 8, and 9.

Finally, we wish to elucidate the importance of retaining $G_2(z)$ in Eq. (24). If G_2 is eliminated from Eq. (24), we violate, for any finite d , the positivity of the curly brackets in Eq. (A1). Consequently $\text{Im } \Sigma(z)$ changes signs both within the upper and lower half planes, as does the imaginary part of $z - \Sigma(z)$. The branch cut $G_{ij}^{(0)}(z)$ possesses on the real axis thus shifts into the upper and lower half planes, and $G_{ij}(z)$ is no longer analytic.

¹ P. G. de Gennes, Phys. Rev. **118**, 141 (1960).

² Y. Nagaoka, Phys. Rev. **147**, 392 (1966).

³ L. N. Bulaevskii, É. L. Nagaev, and D. I. Khomskii, Zh. Eksp. Teor. Fiz. **54**, 1562 (1968) [Sov. JETP **27**, 836 (1968)]; E. L. Nagaev, *Physics of Magnetic Semiconduc-*

tors (MIR, Moscow, 1979).

⁴ W. F. Brinkman and T. M. Rice, Phys. Rev. B **2**, 1324 (1970).

⁵ G. Montambaux, M. Heritier, and P. Lederer, J. Low Temp. Phys. **47**, 39 (1982); P. Kumar and N. S. Sullivan, Phys.

- Rev. Lett. **55**, 963 (1985); Phys. Rev. B **35**, 3162 (1987).
- ⁶ See, for example, R. J. Birgeneau and G. Shirane, *Physical Properties of High Temperature Superconductors* (World Scientific, Singapore, 1989).
- ⁷ For a recent review of the theory, see L. Yu, Z. B. Su, and Y. M. Li, Chin. J. Phys. **31**, 579 (1993).
- ⁸ S. Trugman, Phys. Rev. B **37**, 1597 (1988).
- ⁹ See, e.g., B. I. Shraiman and E. D. Siggia, Phys. Rev. Lett. **60**, 740 (1988); Phys. Rev. B **42**, 2485 (1990).
- ¹⁰ C. L. Kane, P. A. Lee, and N. Read, Phys. Rev. B **39**, 6880 (1989).
- ¹¹ S. Schmitt-Rink, C. M. Varma, and A. E. Ruckenstein, Phys. Rev. Lett. **60**, 2793 (1988).
- ¹² Z. Liu and E. Manousakis, Phys. Rev. B **45**, 2425 (1992).
- ¹³ E. Dagotto, R. Joynt, A. Moreo, S. Bacci, and E. Gagliano, Phys. Rev. B **41**, 9049 (1990).
- ¹⁴ K. J. Szczepanski, P. Horsch, W. Stephan, and M. Ziegler, Phys. Rev. B **41**, 2017 (1990).
- ¹⁵ R. Eder and K. W. Becker, Z. Phys. B **81**, 33 (1990).
- ¹⁶ C. Zhou and H. J. Schultz (unpublished).
- ¹⁷ P. Bénard, L. Chen, and A.-M. S. Tremblay, Phys. Rev. B **47**, 15 217 (1993).
- ¹⁸ T. Tohyama and S. Maekawa, Phys. Rev. B **49**, 3596 (1993).
- ¹⁹ For a comprehensive discussion of the experimental evidence for a next-nearest-neighbor hopping, and previous theoretical studies of the issue, see G. Stemmann, C. Pépin, and M. Lavagna, Phys. Rev. B **50**, 4075 (1994).
- ²⁰ The same problem was recently studied independently by J. Bala, A. M. Olés, and J. Zaanen (unpublished) within the linear-spin-wave, self-consistent Born approximation of Ref. 11.
- ²¹ For a review see D. Vollhardt, in *Perspectives in Many-Particle Physics*, Proceedings of the International School of Physics "Enrico Fermi," Course CXXI, Varenna, 1992, edited by R. A. Broglia and J. R. Schrieffer (North-Holland, Amsterdam, 1994), p. 31.
- ²² W. Metzner, P. Schmit, and D. Vollhardt, Phys. Rev. B **45**, 2237 (1992).
- ²³ R. Strack and D. Vollhardt, Phys. Rev. B **46**, 13 852 (1992).
- ²⁴ R. Strack, Dissertation, TH Aachen, 1993, in *Aachener Beiträge zur Physik kondensierter Materie*, Band 9 (Verlag der Augustinus Buchhandlung, Aachen, 1993).
- ²⁵ E. Müller-Hartmann and C. I. Ventura, Phys. Rev. B **50**, 9235 (1994).
- ²⁶ Q. F. Zhong, S. Sorella, and A. Parola, Phys. Rev. B **49**, 6408 (1994).
- ²⁷ We note that the result for G_{ii} by M. M. Mohan [J. Phys. Condens. Matter **3**, 4507 (1991)] derived on the basis of the retraceable-path approximation is correct even to order $1/d$ and hence coincides with the solution of Eq. (1) at $d = \infty$.
- ²⁸ A. B. Harris and R. V. Lange, Phys. Rev. **157**, 295 (1967).
- ²⁹ For classical spins, zero-temperature antiferromagnetic order will persist at half filling and $d \rightarrow \infty$ throughout the range $t_1^{*2} < t^{*2}/2$. Here t_1^* and t^* are the properly scaled hopping matrix elements [see Eq. (3)].
- ³⁰ D. Forster, *Hydrodynamic Fluctuations, Broken Symmetry and Correlation Functions* (W. A. Benjamin, Reading, MA, 1975), p. 100.
- ³¹ E. Müller-Hartmann, Z. Phys. B **74**, 507 (1989).
- ³² L. Borkowski, A. Schiller, and P. Kumar (unpublished).
- ³³ See, e.g., *Handbook of Mathematical Functions*, edited by M. Abramowitz and I. A. Stegun (Dover, New York, 1972), Chap. 7.
- ³⁴ For $d = 3$, $G_{ij}^{(0)}$ corresponds to a face-centered-cubic lattice. Detailed expressions for this case can be found in T. Morita and T. Horiguchi, J. Math. Phys. **12**, 986 (1971); M. Inoue, *ibid.* **15**, 704 (1974).
- ³⁵ E. Dagotto, A. Nazarenko, and M. Boninsegni, Phys. Rev. Lett. **73**, 728 (1994).